Arabian Journal of Chemistry (2011) 4, 125–134

King Saud University

Arabian Journal of Chemistry

www.ksu.edu.sa
www.sciencedirect.com

REVIEW ARTICLE

Nanorods of transition metal oxalates: A versatile route to the oxide nanoparticles

Tokeer Ahmad [a,*], Aparna Ganguly [a,b], Jahangeer Ahmed [b], Ashok K. Ganguli [b], Omar Abdullah A. Alhartomy [c]

[a] *Nanochemistry Laboratory, Department of Chemistry, Jamia Millia Islamia, New Delhi 110025, India*
[b] *Department of Chemistry, Indian Institute of Technology, Hauz Khas, New Delhi 110016, India*
[c] *Facuty of Science, Department of Physics, University of Tabuk, Tabuk 7149, Saudi Arabia*

Received 23 June 2010; accepted 23 June 2010
Available online 19 August 2010

KEYWORDS

Nanorods;
Nanoparticles;
Reverse micelles;
X-ray diffraction;
Transmission electron microscopy

Abstract A versatile route has been explored for the synthesis of nanorods of transition metal (Cu, Ni, Mn, Zn, Co and Fe) oxalates using reverse micelles. Transmission electron microscopy shows that the as-prepared nanorods of nickel and copper oxalates have diameter of 250 nm and 130 nm while the length is of the order of 2.5 μm and 480 nm, respectively. The aspect ratio of the nanorods of copper oxalate could be modified by changing the solvent. The average dimensions of manganese, zinc and cobalt oxalate nanorods were 100 μm, 120 μm and 300 nm, respectively, in diameter and 2.5 μm, 600 nm and 6.5 μm, respectively, in length. The aspect ratio of the cobalt oxalate nanorods could be modified by controlling the temperature.

The nanorods of metal (Cu, Ni, Mn, Zn, Co and Fe) oxalates were found to be suitable precursors to obtain a variety of transition metal oxide nanoparticles. Our studies show that the grain size of CuO nanoparticles is highly dependent on the nature of non-polar solvent used to initially synthesize the oxalate rods. All the commonly known manganese oxides could be obtained as pure phases from the single manganese oxalate precursor by decomposing in different atmospheres (air, vacuum or nitrogen). The ZnO nanoparticles obtained from zinc oxalate rods are ~55 nm in diameter. Oxides with different morphology, Fe_3O_4 nanoparticles faceted (cuboidal) and Fe_2O_3 nanoparticles (spherical) could be obtained.

* Corresponding author. Tel.: +91 11 26981717x3261; fax: +91 11 26980229.
E-mail address: tokeer.ch@jmi.ac.in (T. Ahmad).

Peer review under responsibility of King Saud University.
doi:10.1016/j.arabjc.2010.06.041

Production and hosting by Elsevier

Contents

1. Introduction

Nanomaterials are among the most challenging areas of current scientific and technological research because of their tremendous possibilities in generating novel shapes, structures and the unusual phenomena associated with these materials (Wadhawan and Multani, 1990). Superior properties have been demonstrated for a broad range of such materials when the size has been reduced to nano-dimension. These nanoscale materials can be defined as those whose characteristic length (at least one length) lies between 1 and 100 nm. The properties of nanomaterials are significantly different from individual atoms or molecules and bulk materials Nanomaterials are exceptionally strong, hard, and ductile at high temperatures, wear resistant, and chemically very active. They exhibit unique electronic, magnetic, optical, photonic and catalytic properties (Lewis, 1993; Alivisatos, 1996) and their size is ideal for use as building blocks (Feldheim and Keating, 1998), which include metals, semiconductors, core–shell nanostructures and organic polymeric materials (McConnell et al., 2000; Trindade et al., 2001; Farmer and Patten, 2001; Xu et al., 2002).

The following effects account for most of the special properties of nanomaterials in contrast to bulk materials; (a) Number of surface atoms, which is a large fraction of the total atoms, makes a distinct contribution to the free energy and results in large changes in the thermodynamic properties of nanocrystals (Murray et al., 1993; Shiang et al., 1996). (b) The intrinsic properties of the nanocrystals are transformed by quantum size effect i.e. changes in the optical and electrical properties with size (Rossetti et al., 1983) arise because of the transformations in the density of electronic energy levels.

Nanowires, nanobelts, nanoribbons, nanosprings and nanorods are a new class of quasi-one-dimensional materials that have attracted considerable interest in the last few years because they offer a unique ability to combine a number of essential diagnostic, imaging, delivery and dosage properties and thus can be functionalized accordingly. For many applications of nanostructured materials or building blocks, the sensitivity or efficiency obtained is directly proportional to the surface area of the material. Nanorods or nanowires possess significantly more surface area than that of the bulk material. Nanorods or nanowires can function as both structural and functional components in devices. Further, nanorods and nanowires can offer unusual physical properties (Cao, 2004; Xia et al., 2003; Rao et al., 2003), and thus find diverse applications in Nanotechnology and specially in the area of biosensors, where a specific molecule is attached to the tip of the nanowire, which then identifies a specific molecule in the living system (Appell, 2002).

The nanowires, which can be grown from a variety of materials and reach tens of micrometers in length, have one major advantage – unlike nanotubes, their chemistry is relatively easy to tailor. The use of nanoscale structures as building blocks for self-assembled (Murray et al., 1995; Mirkin et al., 1996; Alivisatos et al., 1996) structures could potentially eliminate conventional and costly fabrication lines, while still maintaining some concepts that have proven successful in microelectronics. One-dimensional structures, such as nanowires (NWs) and carbon nanotubes (NTs), could be ideal building blocks for nanoelectronics (Hu et al., 1999; Dekker, 1999), because they can function both as devices and as the wires that access them. Electrical transport studies of NTs have yielded data supporting the possibility of field-effect transistors (Tans et al., 1998; Martel et al., 1998), low temperature single-electron transistors (Tans et al., 1997; Bockrath et al., 1997), intramolecular metal–semiconductor diodes (Hu et al., 1999; Yao et al., 1999), and intermolecular-crossed NT–NT diodes (Fuhrer et al., 2000). However, the use of NT building blocks is limited, because the selective growth and/or assembly of semiconducting or metallic NTs (Hu et al., 1999; Dekker, 1999) are not currently possible. Functional nanoscale electronic devices assembled using silicon nanowire building blocks were established by Cui and Lieber (2001). Ultra-long belt-like (or ribbon-like) nanostructures (so-called nanobelts) were successfully synthesized using oxides of zinc, tin, indium, cadmium, and gallium by simply evaporating the desired metal oxide powders at high temperatures (Pan et al., 2001).

Transition metal oxalates have been earlier studied for their thermal decomposition and spectroscopic properties (Gusev et al., 1985; Mohamed et al., 2005). However, these reports have not investigated the possibility of obtaining nanocrystalline transition metal oxides by the thermal decomposition of

the parent oxalates. A previous study on the thermal decomposition of metal oxalates in various atmospheres (air, H_2, and N_2) produces a mixture of their corresponding oxides and no pure phase could be obtained (Mohamed et al., 2005). The oxalate nanorods serve as efficient precursors for obtaining a wide variety of oxide nanoparticles with industrial importance.

The magnetic nano oxide materials have been extensively studied and used in high-density magnetic recording devices, instrumentation and computer data storage, spin valves, ferro-fluid technology, magnetocaloric refrigeration, magnetic resonance imaging (Gleiter, 1989; Gleiter, 2000) and in memory devices (Chakraverty et al., 2005; Sun et al., 2003). When the crystallite sizes are reduced to a few nanometers then single domain particles are more stable which could lead to superparamagnetism and weak ferromagnetism. Another interesting aspect of small-sized magnetic particles is the observation of field reversal due to quantum tunneling (Ibrahim et al., 1995). Copper oxide nanoparticles are of special interest because of their efficiency as nano-fluids in heat-transfer applications. For example, it has been reported that 4% addition of CuO improves the thermal conductivity of water by 20% (Lee et al., 1999).

The magnetic, structural and transport properties of the different manganese oxides are of considerable interest (Nayak and Jena, 1998). These oxides have been used as electrochromic materials and have a wide range of applications in catalysis and battery technologies (Taraseon and Armard, 2001). NiO has been of interest due to its interesting magnetic properties. It is known that bulk crystals of NiO possess a rhombohedral structure and exhibit antiferromagnetic behaviour below 523 K (T_N) and is paramagnetic above that temperature (Smart and Greenwald, 1951). Co_3O_4 is another transition metal oxide of importance because of its application as gas sensors, catalysts, magnetic materials, electrochromic devices and high-temperature solar selective absorbers (Ando et al., 1997; Natile and Glisenti, 2002; Verelst et al., 1999; Maruyama and Arai, 1996; Smith et al., 1980). The dependence of the properties (like band gap) on the size of particles has led to many interesting applications in optical devices of these nanomaterials (Wang and Herron, 1990). ZnO is a wide band gap II–VI semiconductor and used as a phosphor in field emissive displays and in cathodoluminescent devices (Vanheusden et al., 1996; Bachir et al., 1996).

The basic principle for the synthesis of nanoparticles is to inhibit the growth of grains and the stabilization of nanoparticles against aggregation. In the recent past several processes have been developed for the synthesis of nanomaterials, such as mechanical milling, inert gas condensation, and chemical methods such as oxidative precipitation, electrodeposition, hydrothermal and sol–gel synthesis. Among all the chemical processes, which were developed for the preparation of fine functional ceramic powders and for producing a wide array of metals and metal oxide compounds (Sugimoto and Kimijima, 2003; McLeod et al., 2003), the micro-emulsion processing (reverse micelle synthesis) has been demonstrated as a viable method (Ahmad et al., 2005; Ahmad and Ganguli, 2004). This method is superior in terms of being able to deliver homogeneous and monodisperse nanoparticles of a variety of metals, oxides and chalcogenides (Lisiecki and Pileni, 1993; Osseo-Asare and Arriagada, 1990; Koran et al., 1990).

A micro-emulsion system consists of an oil phase, a surfactant and an aqueous phase. It is a thermodynamically stable isotropic dispersion of the aqueous phase in the continuous oil phase. These nanodroplets can be used as nanoreactors to carry out the chemical reactions. Coalescence and de-coalescence among the aqueous droplets lead to the formation of nanoparticles. Besides the droplet size, several other parameters also play an important role in the final size distribution. It has been shown that the micro-emulsion-derived ceramic powders are finer in particle size, narrower in particle size distribution, have easier sinterability and are more homogeneous in composition.

Only few reports are available on the synthesis of nanorods of metal oxalates using the solid state route. Nanorods of copper, cobalt and magnesium oxalate have been prepared by the direct solid state reaction of metal salt and oxalic acid in the presence of surfactant (Cao et al., 2005; Jia et al., 2005; Cao et al., 2005). Single crystal nanoflakes and nanorods of $Ni(OH)_2$, $Co(OH)_2$ and Fe_3O_4 were prepared by a controlled hydrothermal conversion route from $MC_2O_4{\cdot}2H_2O$ in NaOH solution (Li et al., 2003). Wang et al. (2004) synthesized one-dimensional arrays of Co_3O_4 nanoparticles by the thermal treatment of cobalt oxalate nanorods, which were obtained through a convenient solvothermal route.

This review discusses the synthesis of transition metal (Cu, Ni, Mn, Co and Fe) and Zn oxalate nanorods by the reverse micellar route. These oxalate nanorods act as precursors for the synthesis of oxide nanoparticles. The thermal decomposition of these transition metal oxalate rods at low temperatures of 450–500 °C yields homogenous oxide nanoparticles. Our methodology using reverse micelles results in the formation of highly uniform rods of the metal oxalates and not the nanoparticles as obtained in the direct chemical reaction of metal salt and oxalic acid (Xu et al., 2002a,b, 2003). The oxalate nanorods and oxide nanoparticles were characterized in detail by X-ray diffraction, transmission electron microscopy (TEM), atomic force microscopy (AFM), dynamic light scattering (DLS), thermal analysis (TGA/DTA) and Fourier transform infrared spectroscopy (FTIR).

2. Experimental

The synthesis of nanorods has been carried out by mixing the two optically transparent micro-emulsions (**I** and **II**). Micro-emulsion **I** is composed of cetyltrimethylammonium bromide (CTAB) as the surfactant, *n*-butanol as the co-surfactant, iso-octane (or *n*-octane in some cases) as the hydrocarbon phase and aqueous phase containing 0.1 M solution of metal salt (copper nitrate, nickel nitrate, zinc nitrate, manganese acetate, ferrous nitrate and cobaltous nitrate) solution as the aqueous phase. Micro-emulsion **II** comprised the same constituents as mentioned above except for having 0.1 M ammonium oxalate instead of metal salts as the aqueous phase. The weight fractions of various constituents in these micro-emulsions are as follows: 16.76% of CTAB, 13.90% of *n*-butanol, 59.29% of iso-octane and 10.05% of the aqueous phase. These two micro-emulsions were mixed slowly and stirred overnight. The product was separated from the apolar solvent and surfactant by centrifuging and washing it with 1:1 mixture of methanol and chloroform. The precipitate was dried at room temperature.

Metal oxide nanoparticles were obtained by the decomposition of the oxalate precursor at 450–500 °C for 6 h, on the basis of the thermogravimetric studies. CuO nanoparticles were

obtained by the thermal decomposition of copper oxalate monohydrate, synthesized by using both iso-octane and *n*-octane as the non-polar medium. The manganese oxalate nanorods were subjected to a careful thermal decomposition to yield nano-particulate manganese oxides. Anhydrous manganese oxalate was obtained by heating the hydrated precursor at 150 °C. The anhydrous precursor was then heated in air at 450 °C for 6 h to obtain α-Mn_2O_3 and under nitrogen at 500 °C (10 h), Mn_3O_4 was obtained. MnO was obtained by decomposing manganese oxalate in sealed quartz tube at a pressure $\sim 10^{-5}$ torr. The oxides of Ni and Zn were obtained by the decomposition of their metal oxalates in air at 450 °C for 6 h. Nanorods of cobalt and iron oxalate dihydrate were decomposed under different atmospheric conditions (air, helium and hydrogen) to obtain the nanoparticles of various cobalt oxides (Co_3O_4, CoO and metallic Co nanoparticles) and iron oxides (Fe_3O_4 and Fe_2O_3).

Powder X-ray diffraction studies (PXRD) were carried out on a Bruker D8 Advance X-ray diffractometer using Ni-filtered Cu K α radiation. The grain size was calculated using the Scherrer's formula ($t = 0.9\lambda/B \cos\theta$) where t is the diameter of the grain, λ is the wavelength of the radiation (λ for Cu K α is 1.5418 Å) and B is the line broadening which is measured from the broadened peak at full width at half maxima (FWHM) and calculated by Warren's formula; $B^2 = B_M^2 - B_S^2$ where B_M is the full width at half maxima of the sample and B_S is the full width at half maximum of the standard quartz with a grain size of around 2 μm. The cell parameters were determined using a least square fitting procedure on all reflections using quartz as the external standard.

Thermogravimetric (TGA) and differential thermal analyses (DTA) were carried out using Perkin–Elmer TGA and DTA systems on well-ground samples in flowing nitrogen atmosphere with a heating rate of 5 °C/min. Transmission electron microscopic (TEM) studies were carried out using a JEOL JEM 200CX electron microscope operated at 200 kV. TEM specimens were prepared by dispersing the powder in acetone by ultrasonic treatment, dropping onto a porous carbon film supported on a copper grid, and then drying in air.

3. Results and discussion

3.1. Structural analysis of transition metal (Cu, Ni, Mn, Co, Zn and Fe) oxalate nanorods

Using the micro-emulsions containing the metal ions and oxalate ions, we could synthesize metal oxalate at room temperature (Table 1). The powder X-ray diffraction confirmed the formation of pure metal oxalates. The detail of the crystal structure along with the refined cell parameters has been given in Table 2. The PXRD pattern for the orthorhombic Co and Cu oxalate system has been shown in Fig. 1 while monoclinic Ni, Mn, Fe and Zn oxalates are shown in Fig. 2(a–d).

3.2. Thermal studies of transition metal oxalate nanorods

The presence of water molecule in all oxalate nanorods has been confirmed using thermogravimetric and differential thermal analyses (TGA/DTA). All the experiments were carried out in flowing nitrogen. The number of water of crystallization associated with each of these oxalates as calculated from the TGA data and the temperature at which they decompose to give the anhydrous product and then to its corresponding oxide has been tabulated in Table 1.

3.3. Structural analysis of transition metal oxide nanoparticles obtained by the thermal decomposition of transition metal oxalate nanorods

Based on the Thermogravimetric data, the oxalate precursors were decomposed at different temperatures under various conditions to obtain the corresponding oxide nanoparticles. Cop-

Table 1 Details of metal oxalate hydrate ($MC_2O_4{\cdot}nH_2O$) nanorods synthesized using the reverse micellar route.

S. No.	Metal	*n*	Colour	Temperature of decomposition to		Diameter (nm)	Length (nm)
				Anhydrous oxalate (°C)	Oxide (°C)		
1.	Cu	1	Light blue	175	340	130	480
2.	Ni	2	Light green	200	370	250	2500
3.	Mn	2	Grayish white	120	420	100	2500
4.	Zn	2	White	120	400	120	600
5.	Co	2	Light pink	150	380	300	6500
6.	Fe	2	Brown	160	410	70	470

n = number of water molecules.

Table 2 Cell parameters of transition metal oxalate hydrate ($MC_2O_4{\cdot}nH_2O$) nanorods.

S. No.	Metal	Structure	*a* (Å)	*b* (Å)	*c* (Å)	*β*	*n*	JCPDS No
1.	Cu	Orthorhombic	5.47(1)	5.53(2)	2.546(5)	90°	1	21-0279
2.	Ni	Monoclinic	11.77(2)	5.316(7)	9.814(9)	127.19°	2	25-0581
3.	Mn	Monoclinic	12.023(2)	5.646(3)	9.968(7)	128.29°	2	25-0544
4.	Zn	Monoclinic	11.798(6)	5.412(1)	9.873(4)	128.06°	2	25-1029
5.	Co	Orthorhombic	11.826(2)	5.416(7)	15.714(5)	90°	2	25-0250
6.	Fe	Monoclinic	9.915(6)	5.602(4)	9.720(9)	103.9°	2	23-0293
7	Mn	Orthorhombic	7.158(7)	5.873(4)	9.020(9)		0	32-0646

n = number of water molecules.

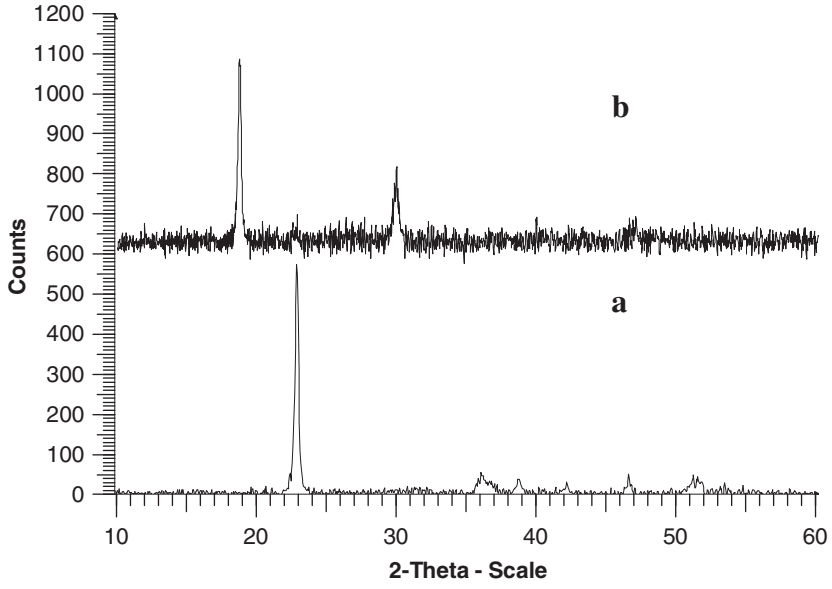

Figure 1 PXRD pattern of (a) copper and (b) cobalt oxalate nanorods.

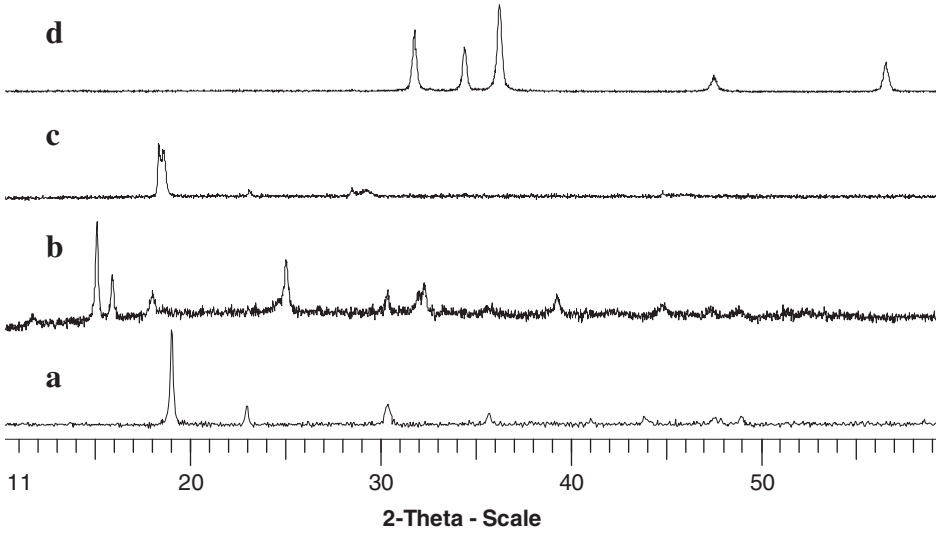

Figure 2 PXRD pattern of (a) Ni (b) Mn (c) Fe and (d) Zn oxalate.

per oxalate monohydrate was heated at 450 °C to obtain pure CuO nanoparticles (using iso-octane as the non-polar solvent) as shown in the PXRD (Fig. 3a). The refined unit cell parameters are $a = 4.684(2)$ Å, $b = 3.4256(7)$ Å, $c = 5.126(3)$ Å, and $\beta = 99.50°$. Pure NiO was obtained after decomposing the nickel oxalate dihydrate precursor in air at low temperature (450 °C) (Fig. 3b), and the refined lattice parameter on the basis of a cubic cell was found to be $a = 4.1743(2)$ Å. Monophasic zinc oxide nanoparticles also obtained by the decomposition of nanorods of zinc oxalate and the PXRD pattern (Fig. 3c) could be indexed on the basis of a hexagonal cell with the refined lattice parameters of $a = 3.2498(4)$ Å and $c = 5.209(1)$ Å which match with the reported pattern of ZnO (Martinez et al., 1993). However, there is a small increase in the c parameter of our nanocrystalline ZnO compared to the bulk value of 5.203(1) Å Reeber, 1970. This may be explained due to the size effect on the lattice parameters. The decrease in the grain size can cause lattice expansion (Duan et al., 2005; Banerjee et al., 2003). This has been explained by the increase in the number of surface atoms of the nanoparticles leading to atomic disorder and reduced coordination of the surface atoms causing the lattice expansion.

Nanorods of manganese oxalate were decomposed under different conditions to obtain oxides in various oxidation states. Pure phases of Mn_2O_3 (Fig. 4a, cubic, $a = 9.425(3)$ Å), Mn_3O_4 (Fig. 4b, tetragonal, $a = 5.7631(9)$ Å, $c = 9.458(3)$ Å) and MnO (Fig. 4c, cubic, $a = 4.4407(5)$ Å) nanoparticles were obtained by heating in air, nitrogen and vacuum, respectively. Similarly nanorods of Cobalt oxalate dihydrate were also decomposed under different conditions (various tempera-

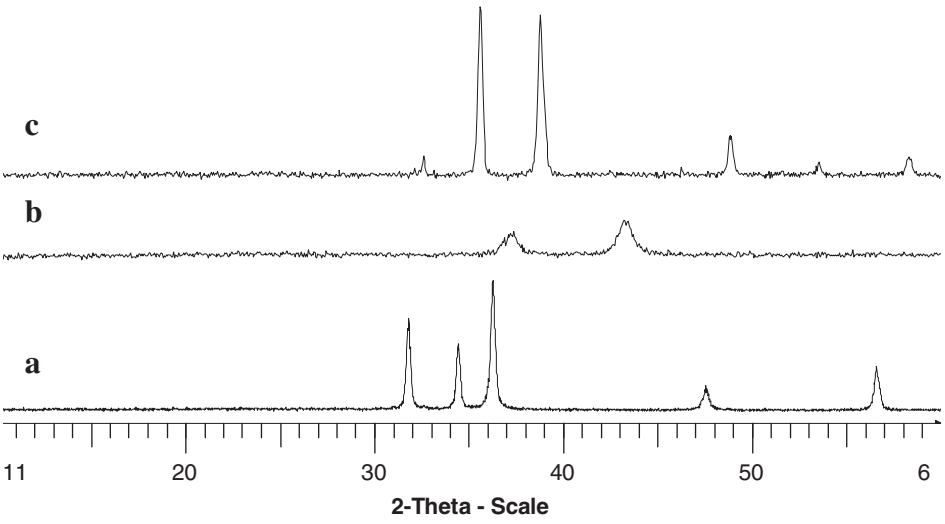

Figure 3 PXRD pattern of (a) CuO (b) NiO (c) ZnO nanoparticles.

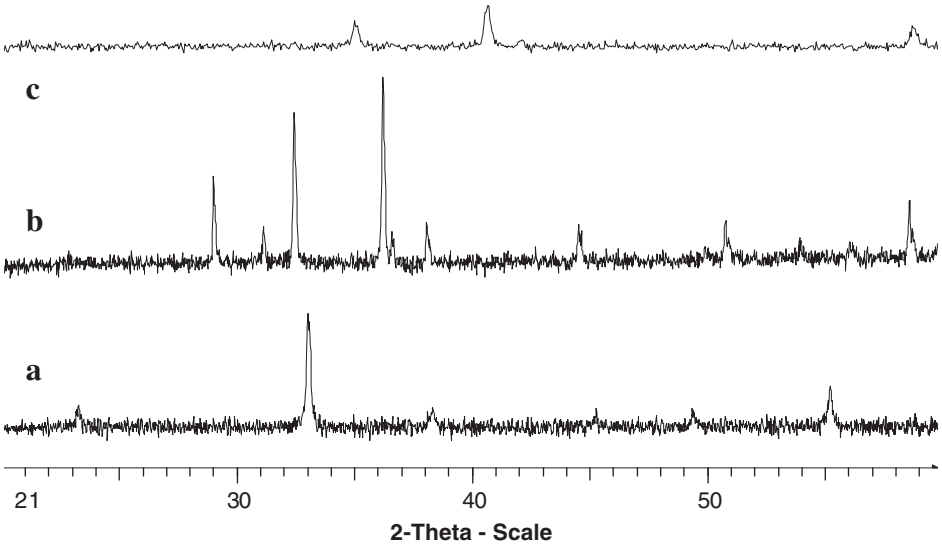

Figure 4 PXRD pattern of (a) MnO, (b) Mn_2O_3 and (c) Mn_3O_4 nanoparticles.

tures and atmospheres) to obtain nanoparticles of cobalt oxides in different oxidation states. On heating the oxalate precursor at 500 °C for 12 h in air, Co_3O_4 nanoparticles were obtained. Powder X-ray diffraction studies show the formation of monophasic Co_3O_4 which could be indexed on the basis of cubic structure (JCPDS No. # 78-1970) with the refined lattice parameter of $a = 8.089(5)$ (Fig. 5). However, a mixture of cobalt oxide (CoO) and Co nanoparticles was obtained from the oxalate precursor when heated in nitrogen or helium atmosphere at 500 °C for 10 h.

Fe_2O_3 nanoparticles have been obtained by decomposing the oxalate precursor at 500 °C in air and confirmed by Powder X-ray diffraction studies (Fig. 6a). It was indexed on the basis of a rhombohedral structure (JCPDS No. # 01-1053) with the refined hexagonal lattice parameters of $a = 5.021(4)$ Å and $c = 13.682(7)$ Å. Another oxide Fe_3O_4 was obtained by decomposing iron oxalate in sealed quartz tube at a pressure $\sim 10^{-5}$ torr. Fig. 6b shows the formation of monophasic Fe_3O_4, which crystallizes in the cubic structure with refined unit cell parameter of $a = 8.381(1)$ Å which is close to the reported value (JCPDS No. 01-1111).

3.4. Grain size analysis of transition metal oxalate nanorods

The dimensions of transition metal oxalate nanorods as obtained by the transmission electron microscopic (TEM) studies have been summarized in Table 1. The average dimensions of the nanorods of copper oxalate monohydrate were 130 nm (diameter) and 480 nm (length) and are more compacted corrugated sheet-like structures (inset of Fig. 7a). These nanorods were obtained with iso-octane as the organic solvent. Interestingly, when the non-aqueous solvent was changed to *n*-octane, rods of slightly different dimension were observed (100 nm in diameter and 640 nm in length) (inset of Fig. 7b) and appeared to be more fibrous. Thus it appears that the solvent plays an important

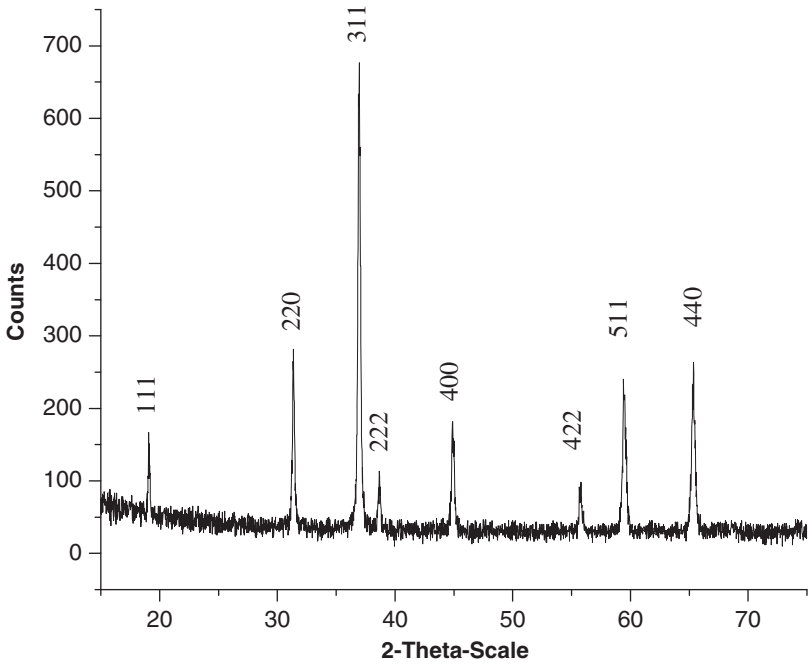

Figure 5 PXRD pattern of Co_3O_4 nanoparticles.

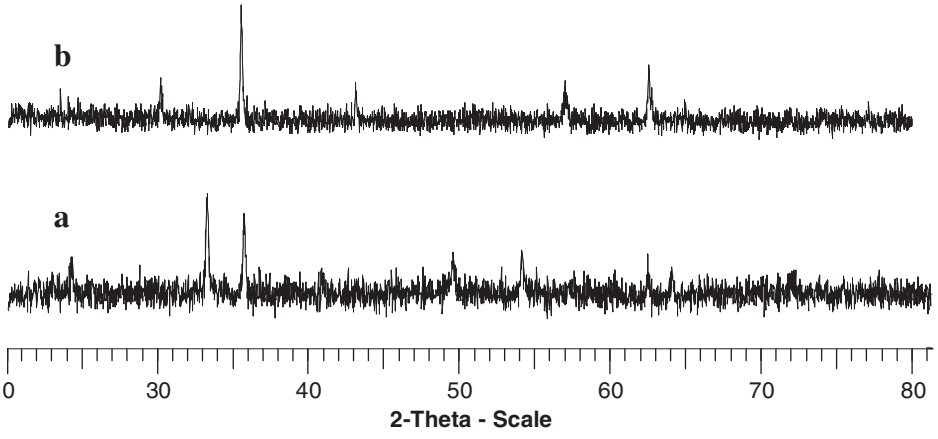

Figure 6 Powder X-ray diffraction patterns of (a) Fe_2O_3 and (b) Fe_3O_4 nanoparticles.

role in controlling the aspect ratio of these nanorods (Ahmad et al., 2005).

The average dimensions of the highly uniform and monodisperse nickel oxalate dihydrate nanorods were found to be 250 nm (diameter) and 2.5 μm (length) (inset of Fig. 8) (Ahmad et al., 2005). TEM studies for anhydrous manganese oxalate show the formation of nanorods (inset of Fig. 9) with average dimensions of 100 nm (diameter) and 2.5 μm (length) Ahmad et al., 2004. Zinc oxalate dihydrate forms nanorods (inset of Fig. 10) with average dimensions of 120 nm (diameter) and 600 nm (length) Ahmad et al., 2006.

TEM studies of cobalt oxalate dihydrate have been performed systematically after heating at various temperatures to see the effect of temperature on the morphology of nanorods of dihydrate and anhydrous cobalt oxalate obtained at room temperature and 185 °C, respectively (Fig. 11). The average diameter of the nanorods remained nearly unchanged at 300 nm till 150 °C while the diameter and length of the anhydrous rods were changed to 100 nm and 1 μm, respectively, at 185 °C (inset of Fig. 11). These nanorods were quite long as compared to nanorods of copper, nickel, manganese and zinc oxalate. The average dimensions of the iron oxalate dihydrate nanorods were 70 nm in diameter and 470 nm in length as shown by the low resolution TEM image (inset of Fig. 12).

3.5. Grain size analysis of transition metal oxide nanoparticles

The oxalate nanorods on decomposition around 450–500 °C led to the formation of oxide nanoparticles. Transmission electron micrographs of the CuO nanoparticles (synthesized using

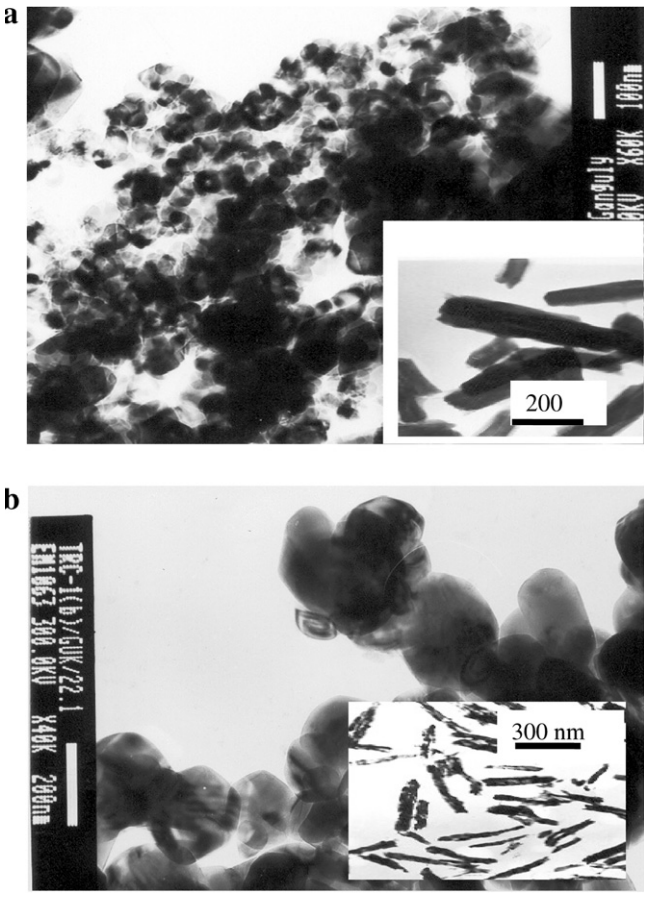

Figure 7 TEM micrograph of CuO nanoparticles synthesized using (a) iso-octane solvent (inset shows the TEM micrographs of corrugated sheet-like structures for the nanorods of copper oxalate) and (b) *n*-octane solvent (inset shows the TEM micrographs for the nanorods of copper oxalate).

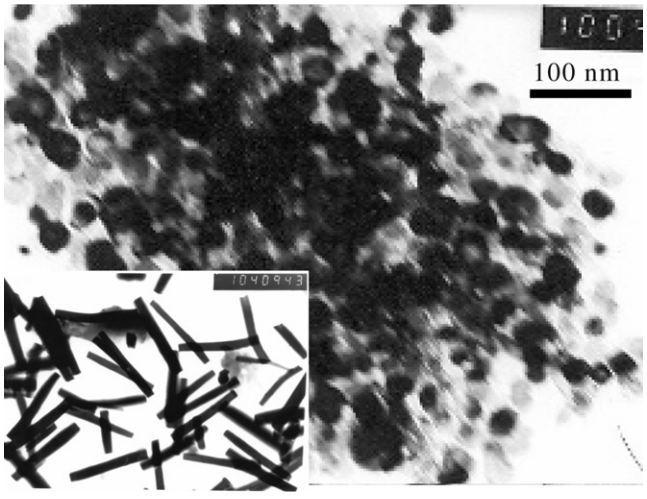

Figure 8 TEM micrograph of NiO nanoparticle. Inset shows the TEM micrographs of nanorods nickel oxalate.

iso-octane as the non-polar solvent) show particles with size in the range of 25–30 nm (Fig. 7a). In contrast, much larger particles of the order of 80–90 nm were obtained from the rods synthesized using n-octane (Fig. 7b). The particles were nearly

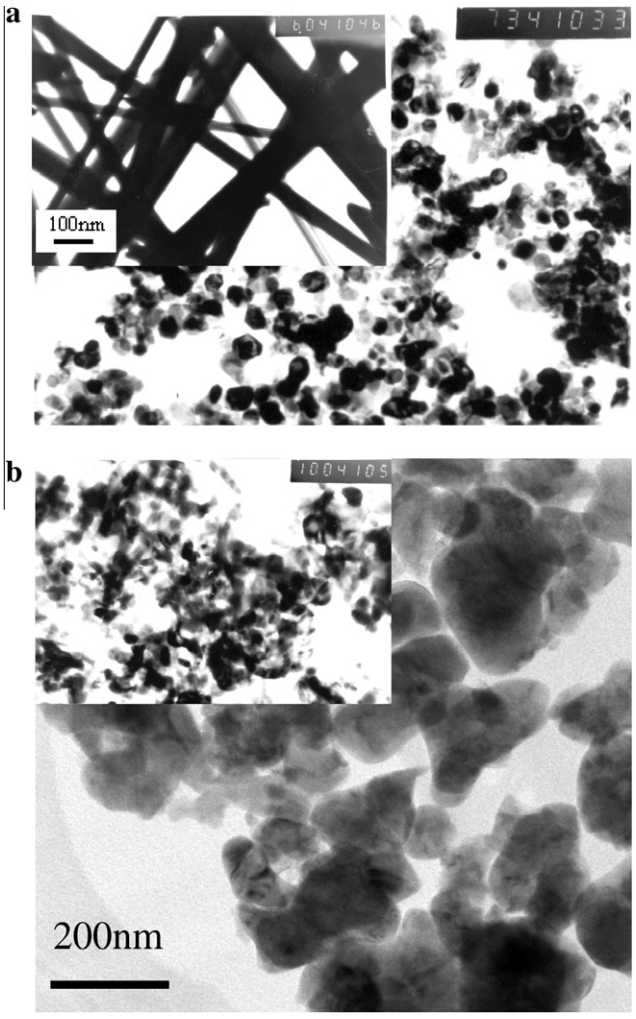

Figure 9 TEM micrograph of (a) MnO (Inset shows the TEM micrographs of nanorods of Mn-oxalate) and (b) Mn_3O_4 nanoparticles (Inset shows the TEM micrographs of Mn_2O_3 nanoparticles).

spherical and showed minimal agglomeration. The grain size of nanostructured nickel oxide was evaluated from X-ray line broadening (using Scherrer's equation) and was found to be 30 nm which is in close agreement with the transmission electron microscopic (TEM) studies with size of ~25 nm (Fig. 8).

X-ray line broadening studies of MnO showed a grain size of 32 nm. TEM studies showed 28 nm sized spherical grains of MnO (Fig. 9a). However, there is a slight increase in the particle size of Mn_2O_3 nanoparticles. From the X-ray diffraction studies, the grain size was evaluated to be 45 nm and that from TEM studies ~50 nm (inset of Fig. 9b), which corroborates the results, obtained from X-ray line broadening studies. Much larger grains (100 nm) were found in the case of Mn_3O_4 nanoparticles (Fig. 9b). It may be noted that there is a gradual increase in particle size from MnO to Mn_3O_4.

The grain size of ZnO nanoparticles was evaluated from X-ray line broadening studies and it was found to be 45 nm. TEM micrograph (Fig. 10) showed spherical particles with close similarity to the XRD results with size ~55 nm. The grain size of Co_3O_4 was found to be 28 nm using X-ray line-broadening studies, while TEM micrograph shows a slightly higher size of 35 nm

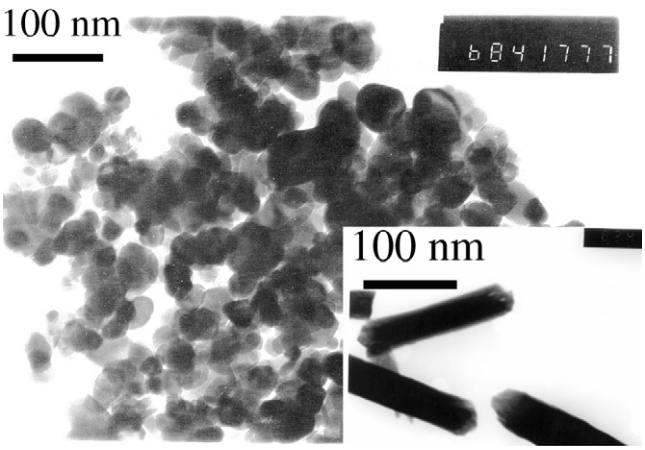

Figure 10 TEM micrograph of ZnO nanoparticles. Inset shows the TEM micrographs of nanorods of Zn-oxalate.

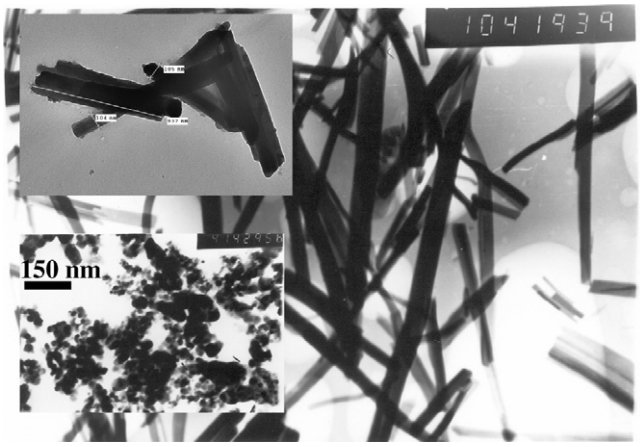

Figure 11 TEM micrograph of nanorods cobalt oxalate dihydrate. Inset shows the TEM micrographs of nanorods of anhydrous cobalt oxalate and Co_3O_4 nanoparticles.

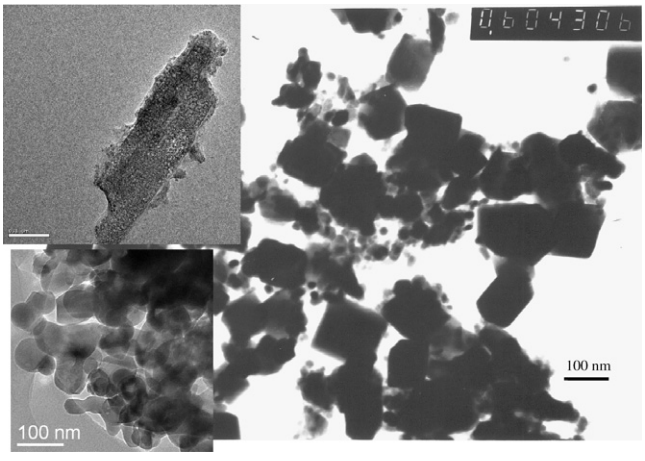

Figure 12 TEM micrograph of Fe_3O_4 nanoparticle. Inset shows the TEM micrographs of nanorods of iron oxalate and Fe_2O_3 nanoparticle.

(inset of Fig. 11). For iron oxide nanoparticles (Fe_2O_3 and Fe_3O_4) with different oxidation states, the line broadening studies gave nearly the same result. The average grain size was found to be 47 nm for Fe_2O_3 and 44 nm for Fe_3O_4. Fe_3O_4 nanoparticles have faceted (cuboidal) grains as shown by TEM micrograph of sizes in the range of 60–70 nm (Fig. 12). On the contrary TEM micrograph in the inset of Fig. 12 shows nearly spherical nanoparticles of Fe_2O_3 of average grain size ~50 nm. Some spherical particles join to form a Y-junction.

4. Conclusions

Synthesis of nanorods of copper oxalate monohydrate, nickel, manganese, zinc, cobalt and iron oxalate dihydrate has been successfully accomplished through the reverse micellar route. The dependence of aspect ratio of the nanorods (copper oxalate monohydrate) on the nature of non-polar solvent could be inferred from the TEM micrographs. The effect of change of oil phase (initially used to synthesize the copper oxalate nanorods) was also reflected in the size of the CuO nanoparticles obtained by the thermal decomposition of the nanorods. Larger (80–90 nm) oxide nanoparticles were observed when straight chain hydrocarbon (*n*-octane) was used as compared to 25–30 nm sized particles obtained from iso-octane (branched chain hydrocarbon). Only copper oxalate crystallizes in the monohydrate and these nanorods appear to be corrugated. All other metal oxalates crystallize as the dihydrate and are smooth. The aspect ratio of the nanorods of cobalt oxalate was temperature dependent. The synthetic route developed for the synthesis of oxalate nanorods is versatile and a large number of monophasic metal oxalate nanorods can be obtained. Nanoparticles of transition metal oxides of copper, nickel, manganese, zinc, cobalt and iron have been obtained successfully by the thermal decomposition of their respective oxalates.

Acknowledgements

TA thanks the Department of Science and Technology (DST) Govt. of India for the financial support and University Grant Commission (UGC) for the special assistance programme to the department. JA and AG thank CSIR Govt. of India for their research fellowship.

References

Ahmad, T., Ganguli, A.K., 2004. J. Mater. Res. 19, 2905.
Ahmad, T., Ramanujachary, K.V., Lofland, S.E., Ganguli, A.K., 2004. J. Mater. Chem. 14, 3406.
Ahmad, T., Kavitha, G., Narayana, C., Ganguli, A.K., 2005. J. Mater. Res. 20, 1415.
Ahmad, T., Chopra, R., Ramanujachary, K.V., Lofland, S.E., Ganguli, A.K., 2005. J. Nanosci. Nanotech. 5, 1840.
Ahmad, T., Vaidya, S., Sarkar, N., Ghosh, S., Ganguli, A.K., 2006. Nanotechnology 17, 1236.
Alivisatos, A.P., 1996. Science 271, 933.
Alivisatos, A.P., Johnsson, K.P., Peng, X., Wilson, T.E., Loweth, C.J., Bruchez, M.P.J., Schultz, P.G., 1996. Nature 382, 609.
Ando, M., Kobayashi, T., Iijima, S., Haruta, M., 1997. J. Mater. Chem. 7, 1779.

Appell, D., 2002. Nature 419, 553.
Bachir, S., Sandouly, C., Kossanyi, J., Ronfard-Haret, J.C., 1996. J. Phys. Chem. Solids 57, 1869.
Banerjee, R., Sperling, E.A., Thompson, G.B., Fraser, H.L., Bose, S., Ayyub, P., 2003. Appl. Phys. Lett. 82, 4250.
Bockrath, M., Cobden, D.H., McEuen, P.L., Chopra, N.G., Zettl, A., Thess, A., Smalley, R.E., 1997. Science 275, 1922.
Cao, G., 2004. J. Phys. Chem. B 108, 19921.
Cao, Y.L., Jia, D.Z., Liu, L., Xiao, D.Q., Xin, X.Q., 2005. Chem. Res. Chin. Univ. 21, 134.
Cao, Y.L., Jia, D.Z., Liu, L., Xiao, D.Q., Xin, X.Q., 2005. Huaxue Xuebao 63, 175.
Chakraverty, S., Bandyopadhyay, M., Chatterjee, S., Dattagupta, S., Frydman, A., Sengupta, S., Sreeram, P.A., 2005. Phys. Rev. B 71, 054401.
Cui, Y., Lieber, C.M., 2001. Science 291, 851.
Dekker, C., 1999. Phys. Today 52, 22.
Duan, Y.W., Kou, X.L., Li, J.G., 2005. Physica B 355, 250.
Farmer, S.C., Patten, T.E., 2001. Chem. Mater. 13, 3920.
Feldheim, D.L., Keating, C.D., 1998. Chem. Soc. Rev. 27, 1.
Fuhrer, M.S., Nygard, J., Shih, L., Forero, M., Yoon, Y.G., Mazzoni, M.S.C., Choi, H.J., Ihm, J., Louie, S.G., Zettl, A., McEuen, P.L., 2000. Science 288, 494.
Gleiter, H., 1989. Prog. Mater. Sci. 33, 223.
Gleiter, H., 2000. Acta Mater. 48, 1.
Gusev, E.A., Dalidovich, S.V., Shandakov, V.A., Vecher, A.A., 1985. Thermochimica Acta 89, 391.
Hu, J., Odom, T.W., Lieber, C.M., 1999. Acc. Chem. Res. 32, 435.
Hu, J., Ouyang, M., Yang, P., Lieber, C.M., 1999. Nature 399, 48.
Ibrahim, M.M., Darwish, S., Seehra, M., 1995. Phys. Rev. B 51, 2955.
Jia, D.Z., Cao, Y.L., Liu, L., Xiao, D.Q., 2005. Wuji Huaxue Xuebao 21, 301.
Koran, A.R., Hull, R., Opila, R.L., Bawendi, M.G., Steigerwald, M.L., Carroll, P.J., Brus, L.E., 1990. J. Am. Chem. Soc. 112, 1327.
Lee, S., Choi, U.S., Li, S., Eastman, J.A., 1999. ASME J. Heat Trans. 121, 280.
Lewis, L.N., 1993. Chem. Rev. 93, 2693.
Li, X.L., Liu, J.F., Li, Y.D., 2003. Mater. Chem. Phys. 80, 222.
Lisiecki, I., Pileni, M.P., 1993. J. Am. Chem. Soc. 115, 3887.
Martel, R., Schmidt, T., Shea, H.R., Hertel, T., Avouris, P., 1998. Appl. Phys. Lett. 73, 2447.
Martinez, O.G., Rojas, R.M., Vila, E., de Vidales, J.L.M., 1993. Solid State Ionics 63, 442.
Maruyama, T., Arai, S., 1996. J. Electrochem. Soc. 143, 1383.
McConnell, W.P., Nowak, J.P., Brousseau, L.C., Fuierer, R.R., Tenent, R.C., Feldheim, D.L., 2000. J. Phys. Chem. B 104, 8925.
McLeod, M.C., McHenry, R.S., Beckman, E.J., Roberts, C.B., 2003. J. Phys. Chem. B 107, 2693.
Mirkin, C.A., Letsinger, R.L., Mucic, R.C., Storhoff, J.J., 1996. Nature 382, 607.
Mohamed, M.A., Galwey, A.K., Halawy, S.A., 2005. Thermochimica Acta 429, 57.
Murray, C.B., Norris, D.B., Bawendi, M.G., 1993. J. Am. Chem. Soc. 115, 8706.
Murray, C.B., Kagan, C.R., Bawendi, M.G., 1995. Science 270, 1335.
Natile, M.M., Glisenti, A., 2002. Chem. Mater. 14, 3090.
Nayak, S.K., Jena, P., 1998. Phys. Rev. Lett. 81, 2970.
Osseo-Asare, K., Arriagada, F.J., 1990. Colloids Surf. 50, 321.
Pan, Z.W., Dai, Z.R., Wang, Z.L., 2001. Science 291, 1947.
Rao, C.N.R., Deepak, F.L., Gundiah, G., Govindaraj, A., 2003. Prog. Solid State Chem. 31, 5.
Reeber, R.R., 1970. J. Appl. Phys. 41, 5063.
Rossetti, R., Nakahara, S., Brus, L.E., 1983. J. Chem. Phys. 79, 1086.
Shiang, J.J., Kadavanich, A., Grubbs, R.K., Alivisatos, A.P., 1996. J. Phys. Chem. 100, 13886.
Smart, J.S., Greenwald, S., 1951. Phys. Rev. 82, 113.
Smith, G.B., Ignatiev, A., Zajac, G., 1980. J. Appl. Phys. 51, 4186.
Sugimoto, T., Kimijima, K., 2003. J. Phys. Chem. B 107, 10753.
Sun, Y., Salamon, M.B., Garnier, K., Averback, R.S., 2003. Phys. Rev. Lett. 91, 167206.
Tans, S.J., Devoret, M.H., Dal, H., Thess, A., Smalley, R.E., Geerligs, L.J., Dekker, C., 1997. Nature 386, 474.
Tans, S.J., Verschueren, R.M., Dekker, C., 1998. Nature 393, 49.
Taraseon, J.M., Armard, M., 2001. Nature 414, 359.
Trindade, T., O'Brien, P., Pickett, N.L., 2001. Chem. Mater. 13, 3843.
Vanheusden, K., Saeger, C.H., Warren, W.L., Tallant, D.R., Voight, J.A., 1996. Appl. Phys. Lett. 68, 403.
Verelst, M.T., Ely, O., Amiens, C., Snoeck, E., Lecante, P., Mosset, A., Respaud, M., Brotom, J.M., Chaudret, B., 1999. Chem. Mater. 11, 2702.
V.K. Wadhawan, M.S. Multani, (1990). Phase transitions, part I and II, special issue on Physics of Clusters and Nanophase Materials, 24–26.
Wang, Y., Herron, N., 1990. Phys. Rev. B 42, 7253.
Wang, X., Chen, X., Gao, L., Zheng, H., Zhang, Z., Qian, Y., 2004. J. Phys. Chem. B 108, 16401.
Xia, Y.N., Yang, P.D., Sun, Y.G., Wu, Y.Y., Mayers, B., Gates, B., Yin, Y.D., Kim, F., Yan, H.Q., 2003. Adv. Mater. 15, 353.
Xu, X.J., Chow, P.Y., Gan, L.M., 2002. J. Nanosci. Nanotech. 2, 61.
Xu, C., Xu, G., Liu, Y., Wang, G., 2002a. Solid State Commun. 122, 175.
Xu, C., Liu, Y., Xu, G., Wang, G., 2002b. Mater. Res. Bull. 37, 2365.
Xu, C., Xu, G., Wang, G., 2003. J. Mater. Sci. 38, 779.
Yao, Z., Postma, H.W.C., Balents, L., Dekker, C., 1999. Nature 402, 273.